DOI: 10.6060/mhc235555s

Novel Glycosylated Cationic Porphyrins: Synthesis, Optical Properties, Singlet Oxygen Generation

Olga M. Kulikova,[a] Alexey V. Lyubimtsev,[b] and Vladimir B. Sheinin[a@]

[a]*G.A. Krestov Institute of Solution Chemistry of the Russian Academy of Sciences, 153045 Ivanovo, Russia*
[b]*Ivanovo State University of Chemistry and Technology, 153000, Ivanovo, Russia*
[@]*Corresponding author E-mail: vbs@isc-ras.ru*

The novel water-soluble porphyrin photosensitizers with meso-(3'-methylpyridyl) and (β-D-galactopyranosyloxy)-phenyl meso-substituents ***H₂P****(3'-MePy⁺)₃(PhG) and* ***H₂P****(3'-MePy⁺)₂(PhG)₂ were synthesized. The comparative study of obtained compounds and cationic* ***H₂P****(3'-MePy⁺)₄ as a standard was carried out. Due to the high hydrophilicity of peripheral substituents all the compounds obtained are highly soluble in aqueous solutions and follow Beer's Law over an operating concentration range. An increase in the fluorescence quantum yield was found with an increase in the number of saccharide fragments. Comparative method based on monitoring the pyridoxine photodegradation in phosphate buffer solution under red light irradiation has been established that the observed rate of pyridoxine decomposition is higher in the presence of* ***H₂P****(3'-MePy⁺)₃(PhG) and* ***H₂P****(3'-MePy⁺)₂(PhG)₂ as compared with* ***H₂P****(3'-MePy⁺)₄, which indicates a higher efficiency of singlet oxygen generation by glycosylated photosensitizers. It was found that the obtained photosensitizers are deprotonated on the porphyrin* ***H₂P*** *platform with close values of stepwise protonation constants, which is accompanied by a significant increase in the intensity of long-wave absorption, fluorescence intensity fluorescence quantum yield of* ***H₂P****(3'-MePy⁺)₃(PhG) and* ***H₂P****(3'-MePy⁺)₂(PhG)₂. It has been shown that the insertion of saccharide fragments shifts the equilibrium of* ***H₂P*** *protonation towards physiological pH values which is the starting point for pH-activation of porphyrin photosensitizers fluorescence in more acidic tumor tissue.*

Keywords: Glycosylated porphyrins, PDT photosensitizers, acid-base properties, singlet oxygen generation, p*H*-dependent fluorescence.

Новые гликозилированные производные катионных порфиринов: синтез, оптические свойства, генерация синглетного кислорода

О. М. Куликова,[a] А. В. Любимцев,[b] В. Б. Шейнин[a@]

[a]*Институт химии растворов им. Г.А. Крестова Российской академии наук, 153045 Иваново, Россия*
[b]*ФГБОУ ВО Ивановский государственный химико-технологический университет, 153000 Иваново, Россия*
[@]*E-mail: vbs@isc-ras.ru*

Синтезированы новые водорастворимые порфириновые фотосенсибилизаторы с мезо-(3'-метилпиридильными) и мезо-(β-D-галактопиранозилокси)фенильными замещителями ***H₂P****(3'-MePy⁺)₃(PhG) и* ***H₂P****(3'-MePy⁺)₂(PhG)₂. Проведено сравнительное исследование полученных соединений и катионного* ***H₂P****(3'-MePy⁺)₄ в качестве стандарта. Благодаря высокой гидрофильности этих мезо-заместителей полученные соединения хорошо растворяются в воде и обладают линейной концентрационной зависимостью поглощения и интенсивности флуоресценции в рабочем диапазоне. Обнаружен рост квантового выхода флуоресценции с увеличением числа сахаридных фрагментов. Методом, основанным на мониторинге фоторазложения пиридоксина в фосфатном буферном растворе при облучении красным светом, установлено, что скорость его деградации выше в присутствии* ***H₂P****(3'-MePy⁺)₃(PhG) и* ***H₂P****(3'-MePy⁺)₂(PhG)₂ по сравнению с* ***H₂P****(3'-MePy⁺)₄, что указывает на более высокую эффективность генерации синглетного кислорода фотосенсибилизаторами с*

сахаридными фрагментами. Установлено, что полученные фотосенсибилизаторы дипротинируются по порфириновой платформе ***H₂P*** *с близкими значениями ступенчатых констант, что сопровождается значительным увеличением интенсивности длинноволнового поглощения, флуоресценции и квантового выхода флуоресценции* ***H₂P****(3'-MePy⁺)₃(PhG) и* ***H₂P****(3'-MePy⁺)₂(PhG)₂. Показано, что введение сахаридных фрагментов смещает равновесия протонирования* ***H₂P*** *в сторону физиологических значений pH, что является отправной точкой для поиска путей pH-активации флуоресценции порфириновых фотосенсибилизаторов в более кислой опухолевой ткани.*

Ключевые слова: Гликолизированные порфирины, фотосенсибилизаторы ФДТ, кислотно-основные свойства, генерация синглетного кислорода, p*H*-зависимая флуоресценция.

Introduction

Tetrapyrrolic macrocycles are widely used as photosensitizers (PSs) in photodynamic therapy (PDT) and photodynamic diagnosis. PSs selectively accumulate in cancerous cells/tissues and after irradiation with a specific red/near infrared light source, a number of photochemical reactions with the production of cytotoxic singlet molecular oxygen and other reactive oxygen species (ROS) are activated in the tumor environment, which leads to destruction of tumor cells. Additionally, PS irradiation with blue light causes its intense fluorescence, which allows to determine the boundaries of the tumor, as well as possible metastases. In modern clinical practice, a number of photosensitizers are used, which vary in their physicochemical, pharmaceutical and pharmacological characteristics, as well as commercial value.[1] Promising PSs should give a clear analytical signal for visualizing the lesion, have high selectivity and phototoxicity against neoplasms of various localization, while remaining safe for healthy tissues and blood cells of the body. Natural and synthetic porphine derivatives due to the unique combination of photophysical and biochemical properties are suitable from this point and therefore widely used as photodynamic PSs.[2–6] It is the current trend to develop effective modification routes of hydrophobic porphyrins for obtaining biocompatible forms of PSs with sufficient water solubility, low toxicity, biological stability, and selectivity. Only biocompatible forms of photosensitizers, which can be delivered with the blood flow to the cancerous lesion, are suitable for PDT. This fact requires chemical modification of hydrophobic tetrapyrrole PSs to provide their water solubility. Chemical modification of porphyrin molecules by introducing cationic, anionic and nonionic hydrophilic groups into macrocycle is widely used for obtaining their water-soluble forms.[7–12] The other problem of developing the ideal PS should be solved is high selectivity to accumulation in target tissue. Promising strategy for target drug delivery is adding the saccharide residues to PS molecules. Early works devoted to porphyrin conjugates with glycoside fragments illustrated improving the solubility of hydrophobic porphyrin molecules and their ability to specific recognition on cell surface.[13–18] Further investigations illustrated the applying a wide range of different synthetic routes[17–24] for production of conjugates with a different hydrophilic/hydrophobic balance and improving cellular uptake of tetrapyrrolic photosensitizers through glycoconjugation with sugar molecules.[18,25–28] Besides, glycosylated macrocycles demonstrated high antimicrobial and antiviral activity,[23,28,29] as well as selectivity to DNA binding.[30] Thus, tetrapyrrolic macrocycles decorated with carbohydrate moieties have a number of advantages for potential use as PDT photosensitizers.[18,31] First, the solubility in water or other biocompatible media, which is a key parameter for medical applications. Second, the possibility to control the degree of glycoporphyrins amphiphilicity and as a sequence, their biodistribution in the body. It is known that cancer cells demonstrated high affinity for glucose through specific protein-transporters ("Warburg effect"),[32–34] the other saccharide residues can also flow into the cell through these specific receptors and that is the third argument in favor of the glycosylated derivatives. A further feature of glycosylated porphyrin derivatives is the chirality of carbohydrate moieties, which provides ability to stereochemical molecular recognition.

Cationic porphyrins are very interesting and perspective objects for PDT applications[35–37] due to, from the one hand, their ability to selective binding and stabilizing G-quadruplexes and inhibit telomerase activity and, from the other, photosensitizing activity in terms of generation of singlet oxygen and other reactive species under light irradiation.[38–42]

Here, we present the synthetic procedure and investigation of chemical and photophysical properties of cationic glycosylated porphyrin derivatives based on 5,10,15,20-tetra(*N*-methylpyridine-3-yl)porphine **H₂P**(3'-MePy⁺)₄: **H₂P**(3'-MePy⁺)₃(PhG) and **H₂P**(3'-MePy⁺)₂(PhG)₂ (Figure 1) as a potential model of photosensitizers for PDT. From some points, porphyrin with cationic N-methylpyridyl groups in the *meta*-positions is more favorable than widely available and well-studied *para*-substituted derivative. For example, *meta*-derivatives are easier to isolate and purified by chromatography at pre-quaternization synthetic step than porphyrins with a cationic groups in *para*-position.[43] Moreover, *meta*-substituted isomer has been demonstrated to be more effective for photodynamic inactivation of multidrug-resistant bacteria.[44] Summarizing, the insertion into the cationic porphyrin macrocycle, which is characterized by high-solubility and photodynamic activity of bulky saccharide moieties, capable of interacting with specific receptors on the cell membrane surface may decrease the undesirable aggregation tendency and provide rapid and selective accumulation of PS in tumor tissues and increase diagnostic and therapeutic efficacy.

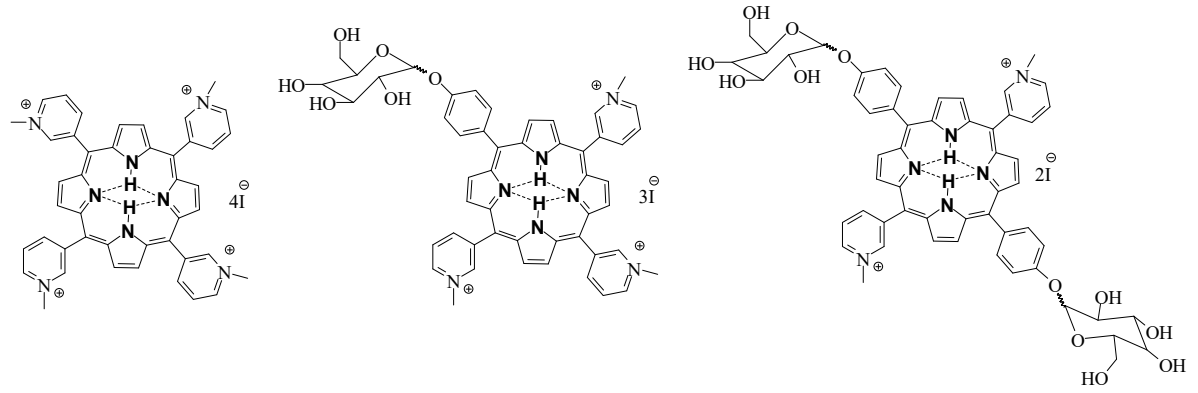

H_2P(3'-MePy$^+$)$_4$ **H_2P**(3'-MePy$^+$)$_3$(PhG) **H_2P**(3'-MePy$^+$)$_2$(PhG)$_2$

Figure 1. Structures of substances under investigation.

Experimental

Chemicals

All commercial reagents were used as received without further purification. The chemicals used for synthetic procedures were of reagent grade quality. The solvents were dried and distilled by standard procedures before use.[45] Phosphate-buffered saline solution p*H* 7.4 (PBS) was prepared using appropriate amounts of Na_2HPO_4 and KH_2PO_4 in double-distilled water. Positively charged 5,10,15,20-tetra(*N*-methylpyridine-3-yl)porphine tetraiodide (**H_2P**(3'-MePy$^+$)$_4$) was synthesized and purified according to procedures presented in literature.[46,47]

Instruments

The absorbance and fluorescence spectra were recorded synchronous at 25C in 1×1 cm optical quartz cell using a fluorescence spectrophotometer (Avantes AvaSpec 2048-2) equipped with a qpod© (Temperature-Controlled Sample Compartment for Fiber Optic Spectroscopy). Micropipette with the scale value is $5.5\cdot10^{-6}$ mL was used for titration experiment. The pH values were measured using InLab Micro pH electrode (Mettler-Toledo Inc.). NMR spectra were recorded on a Bruker Avance III 500 spectrometer (500.17 MHz for 1H) at 294 K. Mass-spectra were recorded on Shimadzu Biotech AXIMA Confidence Linear/Reflectron MALDI-TOF Mass Spectrometer. All samples were run with CHCA and DHB as the matrix or without matrix. Time-resolved photoluminescence measurements in solutions (Time-Correlated Single Photon Counting mode, TCSPC) were performed using FluoTime 300 (Picoquant GmbH) setup, equipped with a diode lasers (450 nm, 40 MHz repetition rate, 100 ps pulse width, Picoquant GmbH; 500 nm, 40 MHz repetition rate, 130 ps pulse width, Picoquant GmbH) as excitation sources. The EasyTau 2 software was used to analyze fluorescence spectra and lifetime decays obtained from FluoTime 300 spectrometer.

Synthesis

4-(2,3,4,6-Tetra-*O*-acetyl-β-D-galactopyranosyl)benzaldehyde was synthesized from 2,3,4,6-tetraacetyl-*O*-acetyl-α-D-galactopyranosyl bromide as described in literature.[24] 5-(Pyridine-3-yl)-dipyrromethane was easily synthesized with nearly quantitative yield from the acid-catalyzed (HCl) condensation of the 3-pyridinecarboxaldehyde and 3 equivalents of pyrrole in water.

5-(4-(β-D-Galactopyranosyloxy)phenyl)-10,15,20-tris(pyridine-3-yl)porphine, ***1b***. Pyrrole (1.8 mL, 26.4 mmol) was added dropwise to a slightly boiling solution of 4-(2,3,4,6-tetra-*O*-acetyl-β-D-galactopyranosyl)benzaldehyde (3.0 g, 6.6 mmol) and 3-pyridinecarboxaldehyde (1.9 mL, 19.8 mmol) in 100 mL propionic acid with 10 mL of acetic anhydride. The reaction mass was boiled for 1.5 hours with air bubbling. After cooling, the solvent was rotary evaporated. The residue was dissolved in methanol, neutralized with an aqueous solution of ammonia, and boiled. Half of the methanol was distilled and diluted with water. The precipitate was filtered and dried in vacuum at 60 °C. The crude product absorbed on aluminum oxide was placed on the top aluminum oxide column and eluted with chloroform and chloroform-methanol mixture (up to 5%). The two bands were collected: the first – 5,10,15,20-tetrakis(pyridine-3-yl)porphine, and second – the mixture of mono- and bis-saccharide porphyrins. The solvent was evaporated to dryness. The residue from second band was dissolved in dry mixture chloroform-methanol, cooled to 0 °C and to this solution the 1 mL of 0.22 M sodium methylate was added dropwise. The solution was stirred for 1 h at room temperature, then five drops of acetic acid was added. The solvent was evaporated to minimal volume, and crude product was purified by column chromatography (silica gel, chloroform-methanol, 5-10%) to give porphyrin **1b**. ^{1}H NMR (500 MHz, DMSO-d_6) δ ppm: 9.39 (s, 3H), 9.07 (dd, J = 5.0, 1.6 Hz, 3H), 8.95 (s, 2H), 8.91–8.80 (m, 6H), 8.67 (bs, 3H), 8.15 (d, J = 7.4 Hz, 2H), 7.97–7.85 (m, 3H), 7.48 (d, J = 8.2 Hz, 2H), 5.39 (d, J = 5.2 Hz, 1H), 5.18 (d, J = 7.7 Hz, 1H), 5.00 (d, J = 5.7 Hz, 1H), 4.78 (t, J = 5.6 Hz, 1H), 4.64 (d, J = 4.6 Hz, 1H), 3.85–3.70 (m, 3H), 3.65 (td, J = 5.6, 3.9 Hz, 2H), 3.60 – 3.50 (m, 1H), –2.95 (s, 2H). MS (MALDI TOF) *m/z*: for $C_{47}H_{37}N_7O_6$ calcd. 795.28; found 797 $[M+2H]^+$.

5,15-bis(4-(β-D-Galactopyranosyloxy)phenyl)-10,20-bis-(pyridine-3-yl)porphine ***2b***. The mixture of 5-(pyridine-3-yl)-dipyrromethane (0.74 g, 3.3 mmol) and 4-(2,3,4,6-tetra-*O*-acetyl-β-D-galactopyranosyl)benzaldehyde (1.5 g, 3.3 mmol) in 40 mL of propionic acid with 4 mL of acetic anhydride was heated and boiled for 1.5 hours with air bubbling. After cooling the solvent was rotary evaporated. The residue was dissolved in methanol, neutralized with an aqueous solution of ammonia, and boiled, then was distilled and diluted with water. The precipitate was filtered and dried in vacuum at 60 °C. The crude product absorbed on aluminum oxide was placed on the top aluminum oxide column and eluted with chloroform and chloroform-methanol mixture (up to 5%). The solvent was evaporated to dryness. The residue was dissolved in dry mixture chloroform-methanol, cooled to 0 °C and to this solution 1 mL of 0.22 M sodium methylate was added dropwise. The solution was stirred for 1 h at room temperature, then five drops of acetic acid was added. The solvent was evaporated to minimal volume, and crude product was purified by column chromatography (silica gel, chloroform-methanol (5-10%)) to give porphyrin **1b** as first band and porphyrin **2b** as second band. ^{1}H NMR (500 MHz, DMSO-d_6) δ ppm: 9.39 (d, J = 2.3 Hz, 2H), 9.06 (dd, J = 4.9, 1.6 Hz, 2H), 8.94 (bs, 4H), 8.83 (bs, 4H), 8.67 (d, J = 7.0 Hz, 2H), 8.15 (d, J = 7.3

Hz, 4H), 7.91 (dd, *J* = 7.7, 5.0 Hz, 2H), 7.48 (d, *J* = 8.3 Hz, 4H), 5.38 (d, *J* = 5.2 Hz, 2H), 5.19 (d, *J* = 7.8 Hz, 2H), 5.00 (d, *J* = 5.6 Hz, 2H), 4.78 (t, *J* = 5.5 Hz, 2H), 4.64 (d, *J* = 4.6 Hz, 2H), 3.85–3.73 (m, 8H), 3.70–3.60 (m, 4H), 3.59 – 3.52 (m, 2H), –2.93 (s, 2H). MS (MALDI TOF) *m/z*: for $C_{54}H_{48}N_6O_{12}$ calcd. 972.33; found 974 $[M+2H]^+$.

*5-(4-(β-D-Galactopyranosyloxy)phenyl)-10,15,20-tris(N-methylpyridine-3'-yl)porphine (**H$_2$P**(3'- MePy$^+$)$_3$(PhG)) and 5,15-bis(4-(β-D-galactopyranosyloxy)phenyl)-10,20-bis(N-methylpyridine-3'-yl)porphine (**H$_2$P**(3'- MePy$^+$)$_2$(PhG)$_2$).* To a stirred solution of porphyrins **1b** or **2b** (0.02 mmol) in freshly distilled DMF 1 mL of methyl iodide was added and the reaction mixture was heated at 95°C for 1.5 h. After the reactions were complete, the porphyrins **H$_2$P**(3'-MePy$^+$)$_3$(PhG) and **H$_2$P**(3'-MePy$^+$)$_2$(PhG)$_2$ were precipitated with benzene. After filtration the compounds were then washed several times with benzene and dried under reduced pressure.

*5-(4-(β-D-Galactopyranosyloxy)phenyl)-10,15,20-tris(N-methylpyridine-3'-yl)porphine **H$_2$P**(3'-MePy$^+$)$_3$(PhG).* ^{1}H NMR (500 MHz, DMSO-d_6) δ ppm: 10.03 (d, *J* = 7.1 Hz, 3H), 9.57 (d, *J* = 5.5 Hz, 3H), 9.44–8.95 (m, 12H), 8.64 (t, *J* = 6.7 Hz, 3H), 8.25 – 8.07 (m, 2H), 7.53 (d, *J* = 8.1 Hz, 2H), 5.22 (d, *J* = 7.7 Hz, 1H), 4.69 (s, 9H), 4.15–3.27 (m, 10H), –3.03 (s, 2H). MS (MALDI TOF) *m/z*: for $[C_{50}H_{46}N_7O_6]^{3+}$ calcd. 841.35; found 841 $[M+H]^+$, 825 $[M-CH_3]^+$.

*5,15-Bis(4-(β-D-galactopyranosyloxy)phenyl)-10,20-bis(N-methylpyridine-3'-yl)porphine **H$_2$P**(3'-MePy$^+$)$_2$(PhG)$_2$.* ^{1}H NMR (500 MHz, DMSO-d_6) δ ppm: 10.02 (d, *J* = 10.5 Hz, 2H), 9.52 (d, *J* = 6.0 Hz, 2H), 9.39 (t, *J* = 7.8 Hz, 2H), 9.10 (bs, 4H), 9.01 (bs, 3H), 8.60 (t, *J* = 7.0 Hz, 2H), 8.14 (d, *J* = 9.5 Hz, 4H), 7.51 (d, *J* = 8.2 Hz, 4H), 5.20 (d, *J* = 7.6 Hz, 2H), 4.66 (s, 6H), 4.03–3.22 (m, 16H), 3.11 (qd, *J* = 7.3, 4.9 Hz, 4H), –2.99 (s, 2H). MS (MALDI TOF) *m/z*: for $[C_{56}H_{54}N_6O_{12}]^{2+}$ calcd. 1002.38; found 1003 $[M+H]^+$, 989 $[M+2H-CH_3]^+$.

Fluorescence quantum yield

Fluorescence quantum yields (Φ_F) were determined by comparative methods,[48] using **H$_2$P**(3'-MePy$^+$)$_4$ (Φ_F = 0.049[49] and **ZnP**(3'-MePy$^+$)$_4$ (Φ_F = 0.017[49]) in water as a standard.

$$\phi_F = \phi_F^{Std} \frac{FA^{Std}n^2}{F^{Std}A(n^{Std})^2},$$

where *F* and F_{Std} are the areas under the fluorescence curves for sample and standard, respectively. *A* and A_{Std} are the absorbances of the sample and reference at the excitation wavelength, respectively. n and n_{Std} are the refractive indices of the solvent used for the sample and standard, respectively.

Singlet oxygen generation

Samples for irradiation were prepared in a 1 cm quartz cells in PBS solution (p*H* = 7.4) with PS concentration *ca.* 10 μM. Each sample was measured at 25 °C with permanent stirring in aerobic conditions. Pyridoxine (150 μM) was used as singlet oxygen sensitive trap. For samples irradiation full spectrum LED (3 W, 175 lm, 3.6 V, 700 mA) installed orthogonally, was used. The 610 nm red glass filter RG-11 was used to cut off undesirable radiation. In all cases, photosensitized oxidation of pyridoxine was controlled by decrease the intensity of the absorption band maximum at 323 nm. UV-Vis spectra were registered in automatic mode every 30 s. The observed photodegradation rate constants (k_{obs}) were calculated by a linear least-squares fit of the semilogarithmic plot of $\ln(A_0/A)$ *vs.* irradiation time.

Results and Discussion

Synthesis

Unsymmetrical porphyrin **1a** with three 3-pyridyls and one protected galactosylated group was prepared following the method of Little *et al.*[50] with a small modification by condensation of 4-(2,3,4,6-tetra-*O*-acetyl-β-D-galactopyranosyl)benzaldehyde (1 eq.) with 3-pyridinecarboxaldehyde (3 eq.) and pyrrole (4 eq.) in propionic acid with 10% acetic anhydride to prevent deacetylation of the glycosylated moiety (Scheme 1).

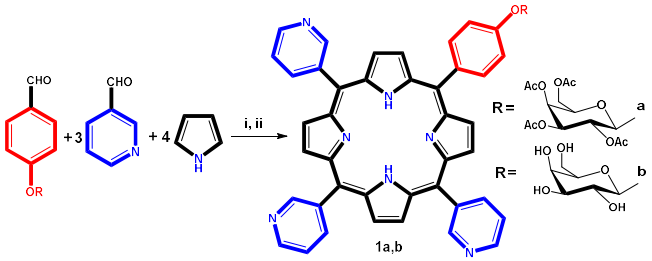

Scheme 1. Synthesis of unsymmetrical porphyrin A_3B-type:
i – propionic acid, reflux; ii – $CHCl_3$-MeOH, MeONa, 0-20 °C.

MS (MALDI TOF) analysis showed the presence of three types of porphyrins: symmetrical 5,10,15,20-tetrakis-(pyridine-3'-yl)porphine (^{1}H NMR spectra and MS MALDI TOF spectra corresponded to the literature data[51]) and two porphyrins with one **1a** and two **2a** saccharide moieties. From this porphyrin mixture only symmetrical porphyrin can be isolated individually by column chromatography (aluminum oxide, silica gel). Mixture of galactosylporphyrins is inseparable in column chromatography experiments. To obtain the porphyrin **1b** a mixture of porphyrins containing carbohydrate substituents was deprotected with a catalytic amount of sodium methylate in a chloroform-methanol mixture. Then desired porphyrin **1b** was isolated by column chromatography on silica gel using chloroform-methanol (5-10%) mixture as eluent. The MS (MALDI TOF) (Figure S1) and ^{1}H NMR (Figure S2) spectra fully confirm the structure of the resulting compound.

Due to the small difference in the mobility of the two porphyrin isomers with two sugar units (ABAB and AABB-types) on the chromatographic column, their separation was unsuccessful. Therefore, for the synthesis of *trans*-bis-galactosylporphyrin **2b** we used 2+2 MacDonald condensation (Scheme 2). To do this, a solution of equimolar amounts of 5-(pyridine-3'-yl)dipyrromethane and 4-(2,3,4,6-tetra-*O*-acetyl-β-D-galactopyranosyl)benzaldehyde was heated in propionic acid in the presence of acetic anhydride under the conditions described above for the synthesis of porphyrin **1b**.

Porphyrin **2b** isolated by column chromatography was a major product with a small amount of porphyrin **1b**, which indicates a slight acidolysis process of dipyrrolylmethane. The $[M+2H]^+$ signal in the spectrum MS (MALDI TOF) (Figure S3) in combination with the

disposition of the β-proton signals in the ^{1}H NMR spectrum (Figure S4) fully confirm the structure of *trans*-porphyrin **2b**.

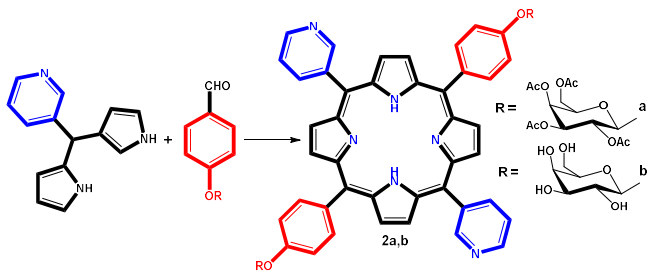

Scheme 2. Synthesis of ABAB-type porphyrin: i – propionic acid, reflux; ii – $CHCl_3$-MeOH, MeONa, 0-20 °C

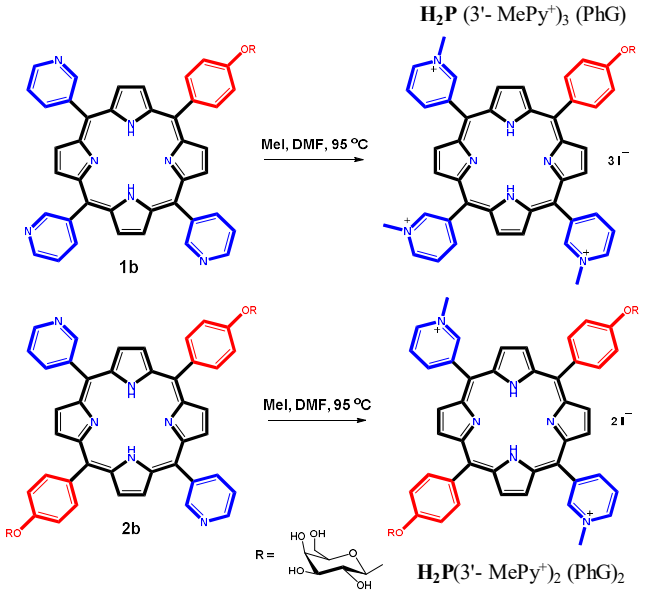

Scheme 3. Synthesis of cationic *N*-methylpyridinium porphyrins H_2P (3'- $MePy^+$)$_3$ (PhG) and H_2P(3'- $MePy^+$)$_2$ (PhG)$_2$.

Finally, tricationic **H_2P**(3'-$MePy^+$)$_3$(PhG) and dicationic **H_2P**(3'- $MePy^+$)$_2$(PhG)$_2$ *N*-methylpyridinium porphyrins were obtained by treatment of galactosylated porphyrins **2a,b** with a large excess of methyl iodide in dry DMF (Scheme 3). These compounds were purified by precipitation in benzene.

In the MS (MALDI TOF) spectra of cationic *N*-methylpyridinium porphyrins **H_2P**(3'-$MePy^+$)$_3$(PhG) and **H_2P**(3'-$MePy^+$)$_2$(PhG)$_2$ (Figure S5) both signals of molecular ion and of a fragment without one methyl group were detected. ^{1}H NMR spectra of porphyrins **H_2P**(3'-$MePy^+$)$_3$(PhG) and **H_2P**(3'-$MePy^+$)$_2$(PhG)$_2$ are generally similar to unmethylated precursors **1b** and **2b**, but have a lower resolution (Figures S6, S7).

Solubility in aqueous solutions

The main problem of most water-soluble porphyrins is their tendency to aggregate in aqueous solutions, which significantly affects the optical properties and is extremely undesirable in their potential use as photosensitizers. Due to the high hydrophilicity of peripheral $MePy^+$ and PhG groups the porphyrin salts **H_2P**(3'-MePyI)$_4$, **H_2P**(3'-MePyI)$_3$(PhG) and **H_2P**(3'-MePyI)$_2$(PhG)$_2$ are very soluble in water with corresponding tetra-, tri- and dications **H_2P**(3'-$MePy^+$)$_4$, **H_2P**(3'-$MePy^+$)$_3$(PhG) and **H_2P**(3'-$MePy^+$)$_2$(PhG)$_2$ formation, and the absorbance and fluorescence of their aqueous solutions are linearly proportional to concentration in the range of 0-5·10^{-6} mol/L (Figure 2, Figure S8-S10, Table 1). Besides, $MePy^+$ and PhG groups are pH-stable in all acidity range of water solutions. All the above have made it possible to undertake a quantitative study of physico-chemical properties of the porphyrin platform in the **H_2P**(3'-$MePy^+$)$_4$, **H_2P**(3'-$MePy^+$)$_3$(PhG) and **H_2P**(3'-$MePy^+$)$_2$(PhG)$_2$ without intra and intermolecular complications.

Table 1. UV-Vis and fluorescence data for synthesized compounds in aqueous solution and PBS.

Compound	UV-Vis					Fluorescence		
	Soret, λ_{max}, nm (lgε)	Q-bands, λ_{max}, nm(lgε)				λ_{max}, nm (λ_{exc}, nm)	Φ_F	τ_F, ns
water								
H_2P (3'-$MePy^+$)$_4$	416(5.43)	514(4.29)	550 (3.71)	580(3.76)	636(2.99)	666, 705(434)	0.049 [49]	7.77
H_4P^{++} (3'-$MePy^+$)$_4$	431(5.51)	579(4.05)		631(4.25)		650 (428)	0.033	2.00
H_2P (3'-$MePy^+$)$_3$(PhG)	418(5.36)	517(4.16)	551(3.63)	581(3.71)	642(3.25)	661, 702 (513)	0.058	7.47
H_4P^{++} (3'-$MePy^+$)$_3$(PhG)	442(5.25)	592(4.02)		643(4.62)		684 (431)	0.093	2.54
H_2P(3'-$MePy^+$)$_2$ (PhG)$_2$	418(5.32)	518(4.04)	554(3.64)	581(3.63)	641(3.37)	661, 702 (513)	0.086	6.74
H_4P^{++} (3'-$MePy^+$)$_2$(PhG)$_2$	446(5.24)	653(4.41)				703 (431)	0.160	2.62
PBS, p*H* 7.4								
H_2P (3'-$MePy^+$)$_4$	416(5.46)	514(4.28)	548(3.61)	581(3.83)	636(2.96)	672, 704 (513)		
H_2P (3'-$MePy^+$)$_3$(PhG)	418(5.40)	517(4.18)	551(3.66)	581(3.75)	641(3.30)	661, 702 (513)		
H_2P(3'-$MePy^+$)$_2$(PhG)$_2$	418(5.32)	518(4.05)	556(3.68)	581(3.65)	642(3.38)	661, 702 (513)		

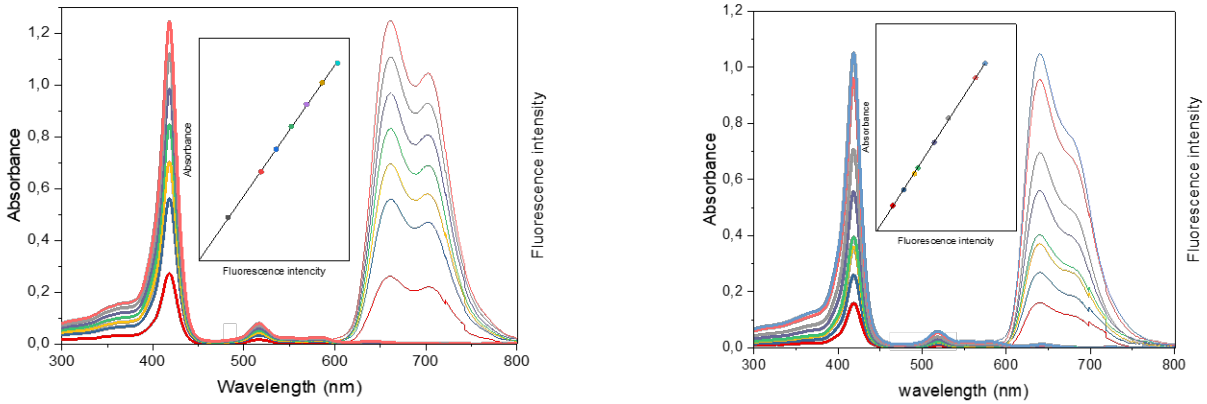

Figure 2. Concentration dependence of absorption (thick lines) and fluorescence (thin lines) spectra of $\mathbf{H_2P}$(3'-MePy$^+$)$_3$(PhG) aqueous solution (C=0-5·10^{-6} M, pH 7, 25ºC) – left; $\mathbf{H_2P}$(3'-MePy$^+$)$_2$(PhG)$_2$ aqueous solution (C=0-5·10^{-6} M, pH 7, 25ºC) -right. Insert: linear correlation between absorbance and fluorescence.

Acid-base properties

Titration of $\mathbf{H_2P}$(3′-MePy$^+$)$_4$, $\mathbf{H_2P}$(3′-MePy$^+$)$_3$(PhG) and $\mathbf{H_2P}$(3′-MePy$^+$)$_2$(PhG)$_2$ solutions with perchloric acid is accompanied by a synchronous pH response in the absorption and fluorescence spectra, which are transformed directly into the spectra of the diprotonated porphyrin platform $\mathbf{H_4P}^{++}$ (Figures 3, 4, S11). The diprotonation leads to a characteristic red shift of the Soret band and an increase in the intensity of the Q1 band, accompanied by a fluorescence enhancement.

For all investigated compounds, the titration curves are smooth, and two families of isosbestic points, corresponding to the extremes of acidity are observed in the UV-Vis spectra, which indicates close values of the constants of the first and second protonation stages.[52–57] The diprotonation of $\mathbf{H_2P}$(3′-MePy$^+$)$_4$, $\mathbf{H_2P}$(3′-MePy$^+$)$_3$(PhG) and $\mathbf{H_2P}$(3′-MePy$^+$)$_2$(PhG)$_2$ in aqueous solution is equilibrium, fast, and very similar to the diprotonation of porphyrin platform in tetraanion of 5,10,15,20-tetrakis(4′-sulfonatophenyl)porphine $\mathbf{H_2P}$(4′-PhSO$_3^-$)$_4$.[53,54] In this case, the loss of the spectral response of the $\mathbf{H_3P}^+$ form is due to the structural and stepwise protonation features of the porphyrin platform. The porphyrin platform $\mathbf{H_2P}$ is formed by two pyrrole rings (A, C) which are the intramolecular hydrogen bond (IMHB) donors and two pyrrolenine rings (B, D) being IMHB acceptors, interconnected by methine bridges (Figure 5).

Cyclization of linear tetrapyrrole into a porphyrin macroheterocycle leads to intramolecular tightness causes the approach of hydrogen and nitrogen atoms at a distance less than the sum of their van der Waals radii (R_w). This intramolecular tightness generates the opposite forces of interatomic hydrogen NH↔HN repulsion and hydrogen NH···N bonding, resulting in the formation of four bifurcated IMHB, which balanced out the intramolecular repulsion and together with the aromatic system, aspire to keep pyrrolenine and pyrrole rings in a coplanar state. The deviation of the interatomic distances NH↔HN and NH···N from the sum of Van der Waals radii is a criterion for the IMHB formation or breaking, respectively. IMHB are formed and forced when downward deviation, but became weaker and break when upward deviation. According to the second Etter's Rule,[58] the four bifurcated IMHB that form six-membered cycles in $\mathbf{H_2P}$ coordination sphere have an advantage over intermolecular hydrogen bonds and blocked $\mathbf{H_2P}$ from interaction with polar solvents and anions.[53,54,59–62]

Protonation of the first pyrrolenine nitrogen atom breaks down two of the four bifurcate IMHB of $\mathbf{H_2P}$, but two others along with aromatic system, aspire to keep two pyrrole and the other pyrrolenine rings of $\mathbf{H_3P}^+$ in the state close to coplanar. The singularity of aromatic tetrapyrrole platforms is the presence of the conventional meso-plane C5C10C15C20, which is only slightly deformed even with a strong distortion of the macrocycle. As a result of intramolecular repulsion between three hydrogens of pyrrole NH-groups, the hydrogen of protonated "B" ring of $\mathbf{H_3P}^+$ (Figure 5) slightly deviates from the *meso*-plane, but the two remaining IMHB still block the $\mathbf{H_3P}^+$ coordination cavity from the intermolecular hydrogen bonds. Further protonation leads to the substitution of IMHB for the intermolecular hydrogen bonding, the perimeter of the aromatic conjugation circuit is expanding, and, as a result, the flexibility of all $\mathbf{H_4P}^{2+}$ platforms increases. Due to intramolecular repulsion between hydrogens of four NH-groups the $\mathbf{H_4P}^{2+}$ acquires a symmetrical 1,3-alternate structure, where hydrogen repulsion forces are balanced by the tendency of the aromatic system to planarity. Diprotonated platform $\mathbf{H_4P}^{2+}$ is a molecular and anion receptor with two identical interdependent cites, pre-organized for binding "guests" with "double-roost" complex formation[62] due to the presence of double positive charge delocalized in annular conjugation circuit and two pairs of converging NH-groups which are hydrogen bond donors. Receptor $\mathbf{H_4P}^{2+}$ is highly complementary with respect to the oxygen atom of a water molecule with a geometric configuration AX$_2$E$_2$.

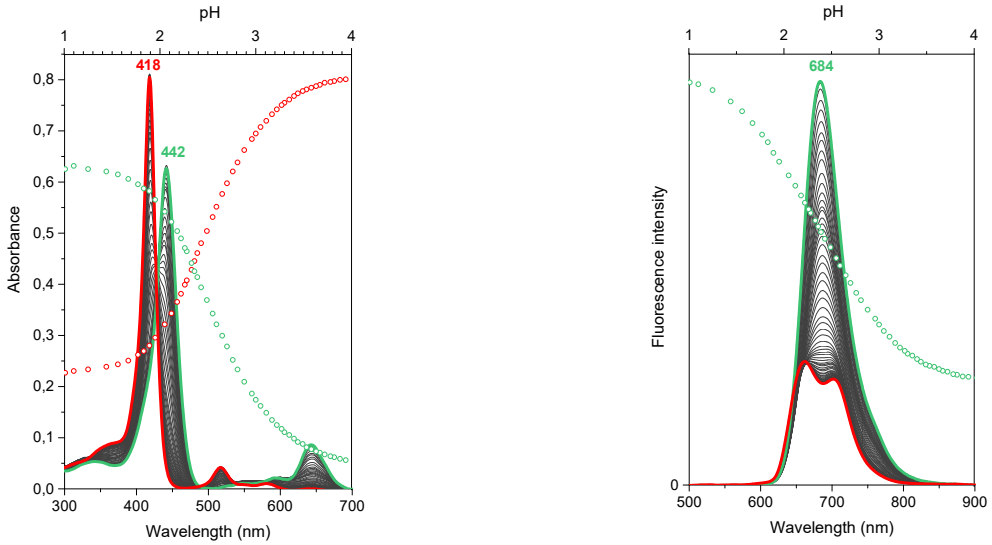

Figure 3. Results of spectropotentiometric titration of $\mathbf{H_2P}$(3′-MePy$^+$)$_3$(PhG) aqueous solution (C=3.5·10^{-6} M, 25°C) with perchloric acid (λ_{exc}=431 nm, the isosbestic point area). Starting spectrum is $\mathbf{H_2P}$(3′-MePy$^+$)$_3$(PhG) form – red line, final spectrum is (H$_2$O)$_2$[$\mathbf{H_4P}^{++}$(3′-MePy$^+$)$_3$(PhG)] form – green line.

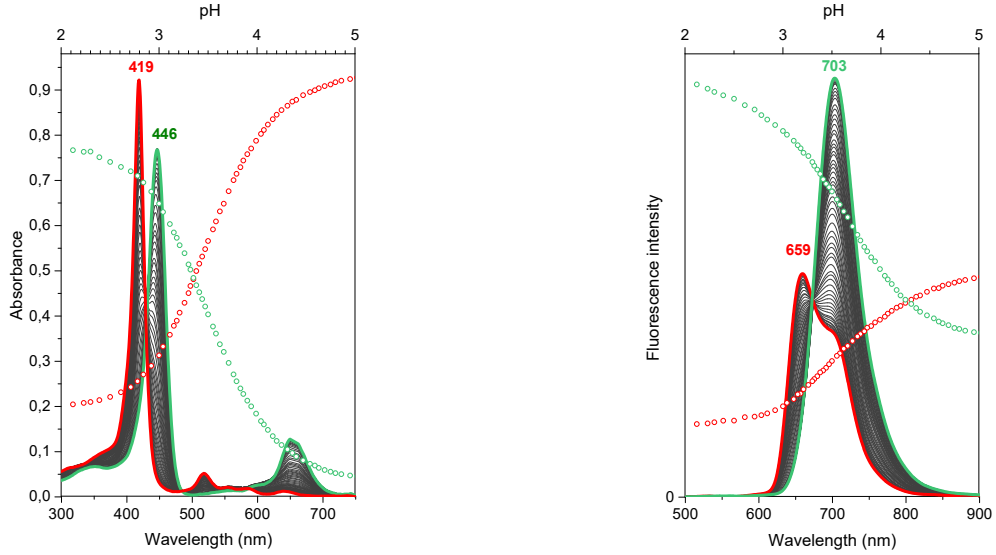

Figure 4. Results of spectropotentiometric titration of $\mathbf{H_2P}$(3′-MePy$^+$)$_2$(PhG)$_2$ aqueous solution (C=4.6·10^{-6} M, 25°C) with perchloric acid (λ_{exc}=431 nm, the isosbestic point area). Starting spectrum is $\mathbf{H_2P}$(3′-MePy$^+$)$_2$(PhG)$_2$ form – red line, final spectrum is (H$_2$O)$_2$[$\mathbf{H_4P}^{++}$(3′-MePy$^+$)$_2$(PhG)$_2$] form – green line.

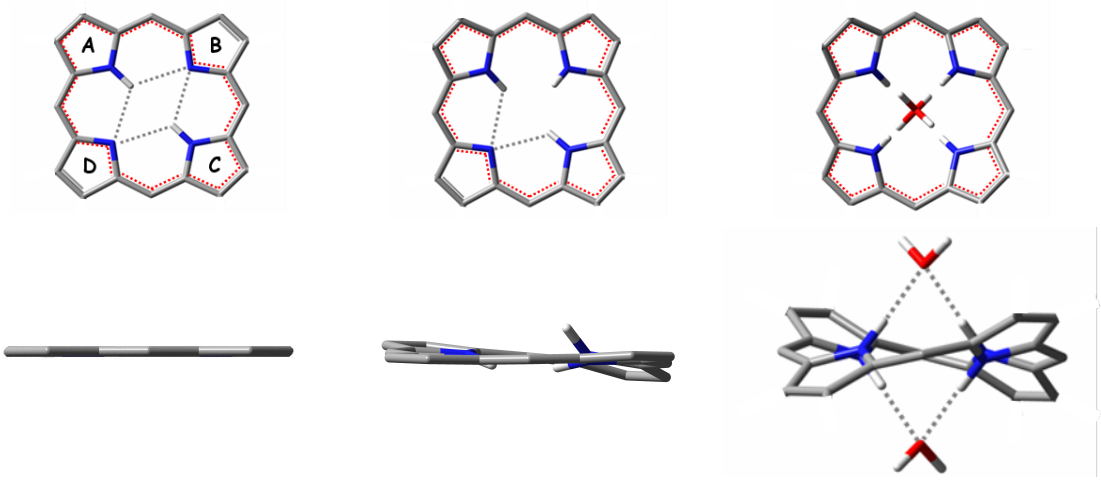

$\mathbf{H_2P}$ $\mathbf{H_3P}^+$ Aquacomplex (H$_2$O)$_2$[$\mathbf{H_4P}^{++}$]

Figure 5. DFT-optimized structure of porphyrin platform $\mathbf{H_2P}$ and its protonated forms $\mathbf{H_3P}^+$ and (H$_2$O)$_2$[$\mathbf{H_4P}^{++}$]. The letters A, B, C and D label the pyrrole and pyrrolenine rings. The 18-electron aromatic cycle is highlighted with a red dotted line, the bifurcated IMHB are highlighted with a gray dotted line. The lower row demonstrates the increasing effect of 1,3-alternation of the tetrapyrrole platform.

Taking into consideration the aquacomplexes formation, protonation equilibria of porphyrin platform in **H$_2$P**(3′-MePy$^+$)$_4$, **H$_2$P**(3′-MePy$^+$)$_3$(PhG) and **H$_2$P**(3′-MePy$^+$)$_2$(PhG)$_2$ can be formally described by the Equations 1-4:

1st protonation stage

$$\mathbf{H_2P} + H^+ \underset{}{\overset{K_{b1}}{\rightleftharpoons}} \mathbf{H_3P}^+ \quad (1)$$

2nd protonation stage

$$\mathbf{H_3P}^+ + H^+ \overset{K_{b2}}{\rightleftharpoons} \mathbf{H_4P}^{++} \quad (2)$$

$$\mathbf{H_4P}^{++} + 2H_2O \overset{K_{(H_2O)_2}}{\rightleftharpoons} (H_2O)_2[\mathbf{H_4P}^{++}] \quad (3)$$

$$\mathbf{H_3P}^+ + H^+ + 2H_2O \overset{K_{b2}\cdot K_{(H_2O)_2}}{\rightleftharpoons} (H_2O)_2[\mathbf{H_4P}^{++}] \quad (4)$$

A huge excess of water, which simultaneously are reagent and solvent (the concentration of water in water is 54.95 mol/L (lgC_{H_2O}=1.74), is the reason for the completely shifted equilibrium of 2nd protonation stage (4) towards [**H$_2$P**$^{++}$](H$_2$O)$_2$, and the optical spectra of diprotonated forms of porphyrins refer to their aqua complexes (H$_2$O)$_2$[**H$_4$P**$^{++}$(MePy$^+$)$_4$], (H$_2$O)$_2$[**H$_4$P**$^{++}$(MePy$^+$)$_3$(PhG)] and (H$_2$O)$_2$[**H$_4$P**$^{++}$ (MePy$^+$)$_2$(PhG)$_2$]. In this case, the experimental constant of the 2nd protonation stage of porphyrins K_{B2} corresponds to the Equation 5:

$$K_{B_2} = K_{b2} \cdot K_{(H_2O)_2} \cdot C_{H_2O}^2 , \quad (5)$$

where C_{H_2O}– concentration of water in water.

The protonation constants K_{b1}, K_{B2} of investigated porphyrins in water (Table 2) were calculated by fitting the parameters in Equation 6 for the experimental titration curves.

Solvation complexes (H$_2$O)$_2$[**H$_4$P**$^{++}$] formation is the reason for a significant decrease of p*H* distance between the protonation stages (1) and (2) amounting to lg$K_{(H_2O)_2}$+2lgC_{H_2O} (3), where $K_{(H_2O)_2}$ is stability constant of (H$_2$O)$_2$[**H$_4$P**$^{++}$] solvation complex and C_{H_2O} is a solvent molar concentration in solution. This "guest"-solvent effect facilitates the addition of only the second proton and thus shrinks the porphyrin diprotonation p*H*-range to higher values. Generally, the convergence of lgK_{b1} and lgK_{B2} (Table 2) is a fair indication of the (H$_2$O)$_2$[**H$_4$P**$^{++}$] complexes formation.[59] The close values of diprotonation constants K_{b1} and K_{B2} are the reason for the two-step titration curves smoothing (Figures 3, 4, S11), the shape of which indicates the shift of the **H$_2$P** (3′-MePy$^+$)$_4$, **H$_2$P**(3′-MePy$^+$)$_3$(PhG) and **H$_2$P**(3′-MePy$^+$)$_2$(PhG)$_2$ 2nd stage protonation equilibrium to the corresponding aquacomplexes (H$_2$O)$_2$[**H$_2$P**(3′-MePy$^+$)$_4$], (H$_2$O)$_2$[**H$_2$P**(3′-MePy$^+$)$_3$(PhG)] and (H$_2$O)$_2$[**H$_2$P**(3′-MePy$^+$)$_2$(PhG)$_2$] formation due to the great excess of the water molecules in aqueous solution.[53,54,59] In the case of **H$_2$P** (3′-MePy$^+$)$_4$ the second proton attached easier than first one as $K_{B2} > K_{b1}$. The probable reason is the abnormally high value of $K_{(H_2O)_2}$ due to the highest positive charge of porphyrin tetra cation. We also noticed some discrepancy in the values of protonation constants, calculated from absorption and fluorescence data, caused by difference in acid-base properties of ground and the excited states of investigated compounds (Table 2). The numerical value of the difference $\lg K_{b1} - \lg K_{B2}$ determines the maximum concentration of the intermediate monoprotonated form [**H$_3$P**$^+$], which affects the shape of the experimental titration curves. Maximum concentration of the monoprotonated form **H$_3$P**$^+$(3′-MePy$^+$)$_4$ reaches 22% at p*H* 1.52, the **H$_3$P**$^+$(3′-MePy$^+$)$_3$(PhG) content is 35% at p*H* 2.52 and **H$_3$P**$^+$(3′-MePy$^+$)$_2$(PhG)$_2$ reaches 35.6% at p*H* 3.38 during the absorption titration, while titration curves are smoothing (Figure 6, Figure S12).

Due to the receptor properties of **H$_4$P**$^{2+}$, it is not possible to isolate and study monoprotonated forms, nevertheless, they should be noted are as stable as the other two forms, involved in the dynamic protolytic equilibria (1) and (2).

$$Y_\lambda = \frac{Y_{0(H_2P)} + Y_{0(H_3P^+)} \cdot K_{b1} \cdot 10^{-pH} + Y_{0((H_2O)_2[H_4P^{++}])} \cdot K_{b1} \cdot K_{B2} \cdot 10^{-2\,pH}}{1 + K_{b1} \cdot 10^{-pH} + K_{b1} \cdot K_{B2} \cdot 10^{-pH}}, \quad (6)$$

where Y_λ – current value of absorbance or fluorescence, Y_{0i} – absorbance or fluorescence of *i*-form solution with analytical porphyrin concentration C_o measured at the wavelength λ.

Table 2. Spectropotentiometric protonation constants lgK_{b1}±0.03 (1) and lgK_{B2}±0.03 (2).

Compound	Absorbance		Fluorescence	
	lgK_{b1}	lgK_{B2}	lgK_{b1}	lgK_{B2}
H$_2$P(3'-PyMe$^+$)$_4$ [63]	1.8	1.3		
H$_2$P(3'-PyMe$^+$)$_4$	1.36	1.88	1.16	1.75
H$_2$P(3'-PyMe$^+$)$_3$(PhG)	2.55	2.49	2.57	1.87
H$_2$P(3'-PyMe$^+$)$_2$(PhG)$_2$	3.47	3.38	3.76	3.35

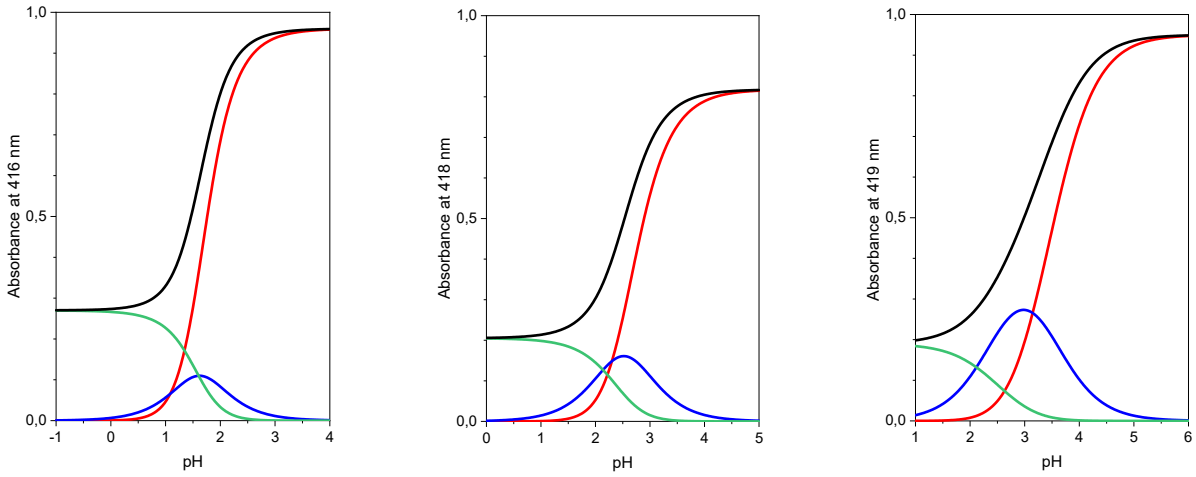

Figure 6. p*H*-Dependent distribution of equilibrium absorption of **H_2P** - red lines, **H_3P^+** - blue lines, $(H_2O)_2$[**H_4P^{++}**] - green lines in water solutions of (a) - **H_2P**(3-$PyMe^+$)$_4$, (b) - **H_2P**(3-$PyMe^+$)$_3$(PhG) and (c) - **H_2P**(3-$PyMe^+$)$_2$(PhG)$_2$ at 25 °C. The resulting experimental titration curve is shown as a dark-green line.

The increase galactose modification of molecular periphery in **H_2P**(3-$PyMe^+$)$_3$(PhG) and **H_2P**(3-$PyMe^+$)$_2$(PhG)$_2$ effects on the macrocycle protonation in solution, so it begins already in the weak-acidic p*H* region, whereas pK values for **H_2P**(3-$PyMe^+$)$_4$ and isomeric **H_2P**(4-$PyMe^+$)$_4$ are extremely small (Table 2).

The disadvantage of photosensitizers with the porphyrin H_2P platform is the low intensity of the red Q_1 absorption band (about 650 nm), which is used in photodynamic theranostics for fluorescence excitation in the "therapeutic window". This circumstance motivates to search for the new forms of tetrapyrrole photosensitizers with more intense absorption and fluorescence in this spectral region.

However, as we can see from Figures 3, 4, S11 porphyrins diprotonation is accompanied by a significant increase in the intensity of long wavelengths absorption and fluorescence. Earlier we have presented results[57] demonstrated the possibility and the concept of p*H*-dependent “off-on” photosensitizers for photodynamic theranostics based on conjugates of tetraphenylporphyrin with nanoparticles of biocompatible polysulfonate Nafion DE 1020, with low fluorescence and phototoxicity in normal tissues and high fluorescence and phototoxicity inside the acidic tumor microenvironment. Diprotonation of PS in these complexes leads to the fluorescence enhancement in the “therapeutic window” spectral region, and the integral intensity even exceeds the value for the PDT drug Fotoditazin®. Insertion in tetrapyrrole macrocycle hydrophilic saccharide groups is another promising way to produce the water-soluble photosensitizers with protolytic equilibrium constant values closer to physiological p*H*. Thus, decrease the p*H* value inside more acidic tumor tissue is the starting point of activated the protonated form of PS, with much more high integral fluorescence as compared with inactive neutral form.

Fluorescence lifetimes and quantum yields

The fluorescence lifetime (τ_F) values were measured for synthesized glycosylated porphyrins and their protonated forms in water. A typical fluorescence decay curves of investigated compounds and their protonated forms are shown in Figure 7. All experimental decays were approximated by biexponential model. Protonated forms of synthesized porphyrins display quenching of the lifetimes as compared with molecular form of porphyrins. In the cases of molecular forms of investigated substances glycosylation of porphyrin macrocycle led to decrease of τ_F values as the number of sugar moieties in molecule increase, but for protonation forms the reverse trend was observed (Table 1). At the same time, the fluorescence quantum yield (Φ_F) for **H_2P**(3'-$MePy^+$)$_2$ (PhG)$_2$ was determined to be 0.086 while that of **H_2P**(3'-$MePy^+$)$_4$ was 0.049 in water. In this case, glycosylation of porphyrin macrocycles led to substantial increase in fluorescence quantum yield. Protonation of porphyrin macrocycle in the case of unsubstituted **H_2P**(3'-$MePy^+$)$_4$ causes quenching the fluorescence, while the protonated forms of glycosylated derivatives demonstrated the significant increase in the values of fluorescence quantum yield, especially in the case of protonated form of **H_2P**(3'-$MePy^+$)$_2$(PhG)$_2$ derivative with two carbohydrate moieties, Φ_F value of which is the highest among investigated photosensitizers (Table 1).

Photostability and singlet oxygen generation

Photostability and the ability to generate highly cytotoxic reactive singlet oxygen are the key parameters for characterization new compounds as potential photosensitizers (PSs). As we have described earlier,[64] the generation of $^1O_2$ was detected indirectly using comparative method, without time-resolved experimental techniques, which require highly sophisticated and expensive equipment. This indirect method involved the analysis of specific substrates photooxidation reaction, determined by the $^1O_2$ consumption method, during the photoexcitation of the given PS.[65] Correspondingly, the substrate concentration decay can be directly related to the amount of generated singlet oxygen. In this study, pyridoxine was chosen as a suitable singlet oxygen sensitive trap and has been used for estimation of photodynamic activity of the substances under study. It should be noticed that indirect methods based on chemical

trapping require the PS light irradiation for a specific period of time, so these methods are suitable only for photostable PS. All synthesized porphyrins remained stable during all irradiation period. The absorption bands of pyridoxine and the studied photosensitizers do not overlap, which provides both selective generation of singlet oxygen and convenient monitoring of pyridoxine photodegradation. The 610 nm red glass filter RG-11 was used to cut off undesirable radiation at the region of pyridoxine and PS absorption, keeping active only the first Q-band of PS (~640 nm) (Figure S13). There were no significant changes in UV-Vis spectra of pyridoxine solution after irradiation with an absence of PS, while PS addition leads to immediate pyridoxine decomposition (Figures 8 and S14).

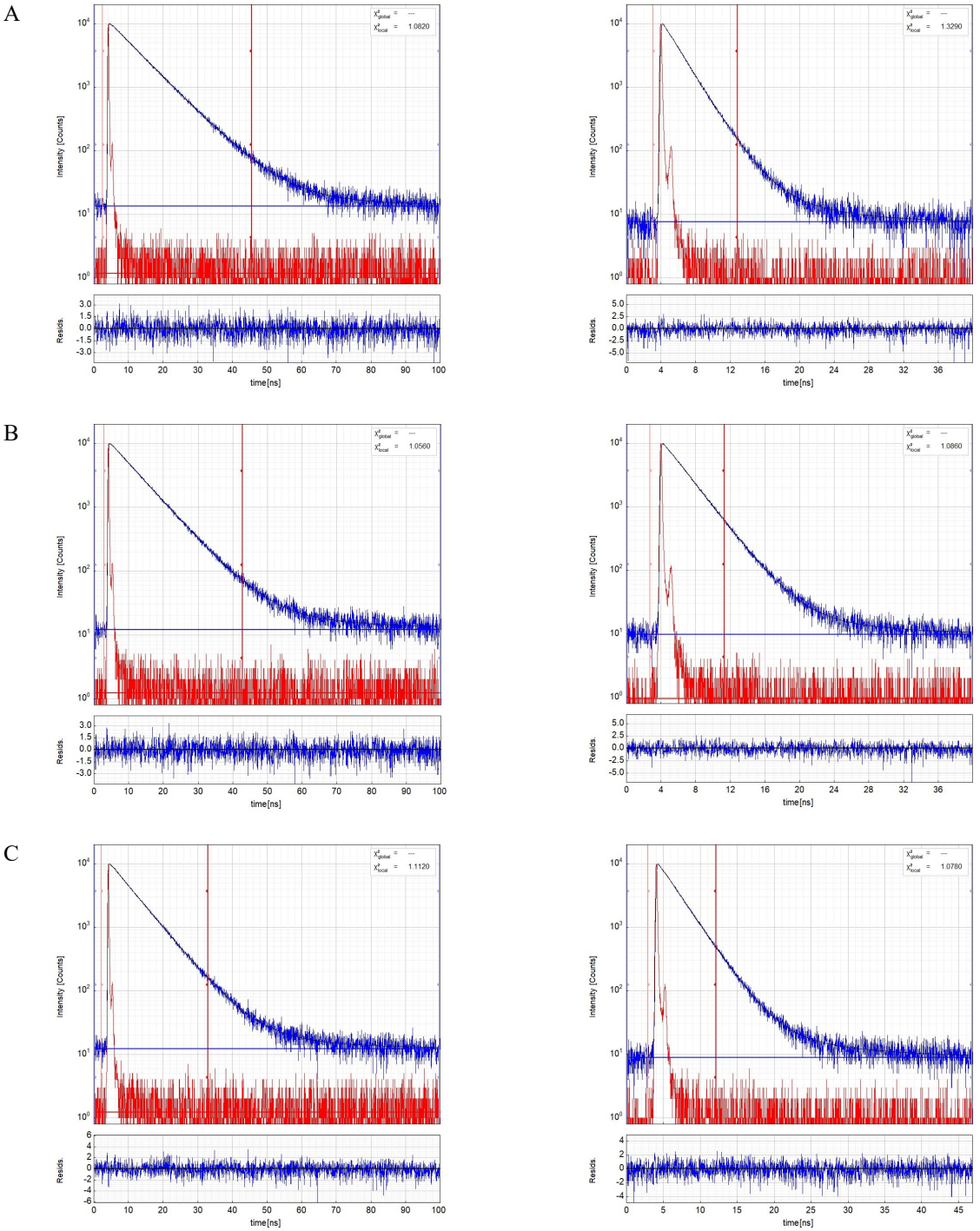

Figure 7. Fluorescence decay curves of (A) – **H$_2$P**(3'-MePy$^+$)$_4$ (left) and **H$_4$P**$^{++}$(3'-MePy$^+$)$_4$ (right), (B) – **H$_2$P**(3'-MePy$^+$)$_3$(PhG) (left) and **H$_4$P**$^{++}$(3'-MePy$^+$)$_3$(PhG) (right), (C) – **H$_2$P**(3'-MePy$^+$)$_2$(PhG)$_2$ (left) and **H$_4$P**$^{++}$(3'-MePy$^+$)$_2$(PhG)$_2$ (right). Solvent – double distilled water.

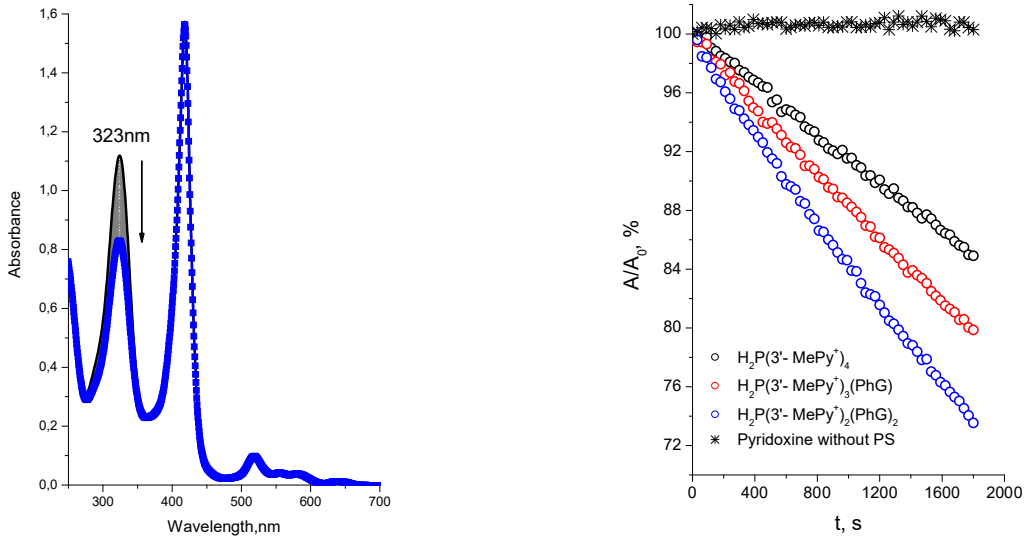

Figure 8. (a)Absorption spectral changes during the irradiation of **H_2P**(3'-$MePy^+$)$_2$ $(PhG)_2$ in PBS with pyridoxine. A cut-off filter RG-11 was used to provide broadband excitation into absorption Q1-band presumably without excitation of other components in solutions. (b) Time-dependent photooxidation of pyridoxine photosensitized by glycosylated porphyrins in PBS monitored at 323 nm.

The observed rate of pyridoxine decomposition is higher in the presence of the all investigated glycosylated derivatives as compared with non-substituted **H_2P**(3'-$MePy^+$)$_4$, which means a higher efficiency of singlet oxygen generation by these photosensitizers under the same experimental conditions (Figures 8, S14, S15a). The sequential glycosylation of porphyrin macrocycle molecules leads to an increase in the observed rate of pyridoxine photodegradation (Figures 8, S14, S15a). A good correlation is observed between the value of the photodegradation rate and the area under the fluorescence curve, which in a good agreement with a higher values of fluorescence quantum yield when increased the number of sugar moieties in molecule (Figure S15b**)**. It is also seen that at the same molar concentrations and excitation conditions, among all investigated compounds the process of pyridoxine photooxidation is faster for photosensitizer **H_2P**(3'-$MePy^+$)$_2$$(PhG)_2$, which also characterized by a higher value of fluorescence quantum yield (Table 1).

Conclusions

The construction of water-soluble porphyrin PS with cationic 3′-methylpyridyl and saccharide fragments having a high affinity for cancer cells is a promising strategy for providing target delivery of phototoxic drugs to tumor tissues. Obtained and studied in this work target compounds **H_2P**(3'-$MePy^+$)$_3$(PhG) and **H_2P**(3'-$MePy^+$)$_2$$(PhG)_2$ demonstrate a higher ability to singlet oxygen generation as compared with **H_2P**(3'-$MePy^+$)$_4$ used as a standard. The advanced research direction is the development of glycosylated PS capable of protonating inside a more acidic tumor tissue on a porphyrin platform to the **H_2P^{++}** dication with much more intense integral fluorescence compared to **H_2P**.

Acknowledgements. This work was supported by RSF (Russian Science Foundation) according to the research project № 23-23-00491, https://rscf.ru/en/project/23-23-00491/. Equipment of the Shared Facility Center, the Upper Volga Regional Center of Physicochemical Studies was used.

References

1. Habermeyer B.G.R. *Photochem. Photobiol. Sci.* **2018**, *17*, 1675–1690, doi: 10.1039/C8PP00222C.
2. Ethirajan M., Chen Y., Joshy P.P.R. *Chem. Soc. Rev.* **2011**, *40*, 340–362, doi: 10.1039/B915149B.
3. Li H., Xiao W., Tian Z., Liu Z., Shi L., Wang Y. *Photodiagnosis Photodyn. Ther.* **2023**, *41*, 103236, doi: 10.1016/j.pdpdt.2022.103236.
4. Guterres K.B., Rossi G.G., de Campos M.M.A, Moreira K.S., Burgo T.A.L., Iglesias B.A. *Photodiagnosis Photodyn. Ther.* **2022**, *38*, 102770, doi: 10.1016/J.PDPDT.2022.102770.
5. Hou B., Zhang W., Li C., Sun X., Feng X., Liu J. *Appl. Organomet. Chem.* **2022**, *36*, e6598, doi: 10.1002/AOC.6598.
6. Makola L.C., Nwahara N., Managa M., Nyokong T. *J. Coord. Chem.* **2022**, *75*, 1112–1128, doi: 10.1080/00958972.2022.2087515.
7. Luciano M.B.C. *Molecules* **2017**, *22*, 980, doi: 10.3390/molecules22060980.
8. Babu B., Soy R.C., Mack J., Nyokong T. *New J. Chem.* **2020**, *44*, 11006–11012, doi: 10.1039/D0NJ01564D.
9. Cui X., Li Y., Li Y., Qiu B., Duan Q. *Dyes Pigm.* **2019**, *164*, 237–243, doi: 10.1016/J.DYEPIG.2019.01.034.
10. Bonsall S., Hubbard S., Jithin U., Anslow J., Todd D., Rowding C. *Cancers (Basel)* **2022**, *14*, 5446, doi: 10.3390/CANCERS14215446/S1.
11. Hilmey D.G., Abe M., Nelen M.I., Stilts C.E., Baker G.A., Baker S.N. *J. Med. Chem.* **2002**, *45*, 449–461, doi: 10.1021/JM0103662/SUPPL_FILE/JM0103662_S.PDF.
12. Zhang W.Y., Li G.C., Li Y.Y., Fan Y., Sun X.Q., Zhang Q.B., Hou B.J., Xu W.B., Jin N.Z., Feng X.X., Liu J.Ch. J. *Porphyrins Phthalocyanines* **2022**, *26*, 384–391, doi: 10.1142/S1088424622500304.

13. Fülling G., Schröder D., Franck B. *Angew. Chem. Int. Ed. English* **1989**, *28*, 1519–1521, doi: 10.1002/ANIE.198915191.
14. Fujimoto K., Miyata T., Aoyama Y. *J. Am. Chem. Soc.* **2000**, *122*, 3558–3559, doi: 10.1021/JA993993D/ASSET/IMAGES/LARGE/JA993993DF00002.JPEG.
15. Maillard P., Guerquin-Kern J.L., Momenteau M., Gaspard S. *J. Am. Chem. Soc.* **1989**, *111*, 9125–9127, doi: 10.1021/JA00207A033/ASSET/JA00207A033.FP.PNG_V03.
16. Driaf K., Krauzz P., Verneuil B., Spiro M., Blais J.C., Bolbach G. *Tetrahedron Lett.* **1993**, *34*, 1027–1030, doi: 10.1016/S0040-4039(00)77483-1.
17. Driaf K., Granet R., Krausz P., Kaouadji M., Thomasson F., Chulia A.J. *Can. J. Chem.* **1996**, *74*, 1550–1563, doi: 10.1139/v96-172.
18. Aksenova A.A., Sebyakin Y.L., Mironov A.F. *Russ. J. Bioorg. Chem.* **2003**, *29*, 201–219, doi: 10.1023/a:1023924213863.
19. Maillard P., Huel C., Momenteau M. *Tetrahedron Lett.* **1992**, *33*, 8081–8084, doi: 10.1016/S0040-4039(00)74723-X.
20. Cavaleiro J.A.S., Tomé J.P.C., Faustino M.A.F. In: *Heterocycles from Carbohydrate Precursors. Topics in Heterocyclic Chemistry* (El Ashry E.S.H., Ed.), Berlin: Springer, **2007**, doi: 10.1007/7081_2007_056.
21. Bennion M.C., Burch M.A., Dennis D.G., Lech M.E., Neuhaus K., Fendler N.L. *Eur. J. Org. Chem.* **2019**, 6496–6503, doi: 10.1002/ejoc.201901128.
22. Silva S., Pereira P.M.R., Silva P., Almeida Paz F.A., Faustino M.A.F., Cavaleiro J.A.S. *Chem. Commun.* **2012**, *48*, 3608–3610, doi: 10.1039/c2cc17561d.
23. Tomé J.P.C., Silva E.M.P., Pereira A.M.V.M., Alonso C.M.A., Faustino M.A.F., Neves M.G.P.M.S. *Bioorg. Med. Chem.* **2007**, *15*, 4705–4713, doi: 10.1016/j.bmc.2007.05.005.
24. Oulmi D., Maillard P., Guerquin-Kern J.L., Huel C., Momenteau M. *J. Org. Chem.* **1995**, *60*, 1554–1564, doi: 10.1021/ jo00111a013.
25. Tracy E.C., Joshi P., Dukh M., Durrani F.A., Pandey R.K., Baumann H. *J. Porphyrins Phthalocyanines* **2023**, *27*, 1164–1176, doi: 10.1142/S1088424623500657.
26. Pereira P.M.R., Silva S., Ramalho J.S., Gomes C.M., Girão H., Cavaleiro J.A.S. *Eur. J. Cancer* **2016**, *68*, 60–69, doi: 10.1016/j.ejca.2016.08.018.
27. Samaroo D., Zahran M., Wills A.C., Guevara J., Tatonetti A. *J. Porphyrins Phthalocyanines* **2019**, *23*, 437–452, doi: 10.1142/S1088424619500275.
28. Singh S., Aggarwal A., Bhupathiraju N.V.S.D.K., Arianna G., Tiwari K., Drain C.M. *Chem. Rev.* **2015**, *115*, 10261–10306, doi: 10.1021/acs.chemrev.5b00244.
29. Fernández L., Lin Z., Schneider R.J., Esteves V.I., Cunha Â., Tomé J.P.C. *ChemPhotoChem* **2018**, *2*, 596–605, doi: 10.1002/cptc.201700169.
30. Lebedeva N.S., Yurina E.S., Guseinov S.S., Gubarev Y.A., Syrbu S.A. *Dyes Pigm.* **2019**, *162*, 266–271, doi: 10.1016/j.dyepig.2018.10.034.
31. Titov D. V, Gening M.L., Tsvetkov Y.E., Nifantiev N.E. *Russ. Chem. Rev.* **2014**, *83*, 523–554, doi: 10.1070/RC2014V083N06ABEH004426/XML.
32. Warburg O. *Science* **1956**, *123*, 309–314, doi: 10.1126/science.123.3191.309
33. Kim J.W., Dang C. V. *Cancer Res.* **2006**, *66*, 8927–8930, doi: 10.1158/0008-5472.CAN-06-1501.
34. Pereira P.M.R., Berisha N., Bhupathiraju N.V.S.D.K., Fernandes R., Tomé J.P.C., Drain C.M. *PLoS One* **2017**, *12*, 1–21, doi: 10.1371/journal.pone.0177737.
35. Carneiro J., Gonçalves A., Zhou Z., Griffin K.E., Kaufman N.E.M., da Vicente M.G.H. *Lasers Surg. Med.* **2018**, *50*, 566, doi: 10.1002/LSM.22824.
36. Garcia-Sampedro A, Tabero A, Mahamed I, Acedo P. *J Porphyrins Phthalocyanines* **2019**, *23*, 11–27, doi: 10.1142/S1088424619500111.
37. Rapozzi V, Zorzet S, Zacchigna M, Della Pietra E, Cogoi S, Xodo L.E. *Mol. Cancer* **2014**, *131*, 1–17, doi: 10.1186/1476-4598-13-75.
38. Caterino M., D'Aria F., Kustov A.V., Belykh D.V., Khudyaeva I.S., Starseva O.M. *Int. J. Biol. Macromol.* **2020**, *145*, 244–251, doi: 10.1016/J.IJBIOMAC.2019.12.152.
39. Lebedeva N.S., Yurina E.S., Gubarev Y.A., Syrbu S.A. *Spectrochim. Acta Part A Mol. Biomol. Spectrosc.* **2018**, *199*, 235–241, doi: 10.1016/J.SAA.2018.03.066.
40. Mathew D., Sujatha S. *J. Inorg. Biochem.* **2021**, *219*, 111434, doi: 10.1016/J.JINORGBIO.2021.111434.
41. Palma E., Carvalho J., Cruz C., Paulo A. *Pharm.* **2021**, *14*, 605, doi: 10.3390/PH14070605.
42. Sanchez-Martin V., Soriano M., Garcia-Salcedo J.A. *Cancers* **2021**, *13*, 3156, doi: 10.3390/CANCERS13133156.
43. Lebedeva N.S., Yurina E.S., Guseinov S.S., Gubarev Y.A. *Dyes Pigm.* **2023**, *220*, 111723, doi: 10.1016/J.DYEPIG.2023.111723.
44. Schulz S., Ziganshyna S., Lippmann N., Glass S., Eulenburg V., Habermann N. *Microorganisms* **2022**, *10*, 858, doi: 10.3390/microorganisms10050858.
45. Armarego W.L.F. *Purification of Laboratory Chemicals*. Butterworth-Heinemann, **2017**, doi: 10.1016/s0022-328x(00)82974-5.
46. Le Roux D., Mialocq J.C., Anitoff O., Folcher G. *J. Chem. Soc. Faraday Trans. 2 Mol. Chem. Phys.* **1984**, *80*, 909–920, doi: 10.1039/F29848000909.
47. Berezin M.B., Berezina N.M., Bazanov M.I., V'yugin A.I., Semeikin A.S., Glazunov A.V. *Russ. J. Phys. Chem. A* **2010**, *84*, 1449–1451, doi: 10.1134/S0036024410080303.
48. Managa M., Ngoy B.P., Nyokong T. *J. Photochem. Photobiol. A Chem.* **2017**, *339*, 49–58, doi: 10.1016/J.JPHOTO CHEM.2017.02.018.
49. Kalyanasundaram K. *Inorg. Chem.* **1984**, *23*, 2453–2459, doi: 10.1021/ic00184a019.
50. Little R.G., Anton J.A., Loach P.A., Ibers J.A. *J. Heterocycl. Chem.* **1975**, *12*, 343–349, doi: 10.1002/JHET .5570120226.
51. Lyubimtsev A.V., Semeikin A.S., Koifman M.O., Koifman O.I. *Dokl. Chem.* **2023**, *508*, 13–22, doi: 10.1134/S0012500823600128/FIGURES/11.
52. Sheinin V.B., Kulikova O.M., Koifman O.I. *J. Mol. Liq.* **2019**, *277*, 397–408, doi: 10.1016/j.molliq.2018.12.105.
53. Sheinin V.B., Shabunin S.A., Bobritskaya E.V., Koifman O.I. *Macroheterocycles* **2011**, *4*, 80–84, doi: 10.6060/mhc2011.2.02.
54. Sheinin V.B., Shabunin S.A., Bobritskaya E.V., Ageeva T.A., Koifman O.I. *Macroheterocycles* **2012**, *5*, 252–259, doi: 10.6060/mhc2012.120989S.
55. Sheinin V.B., Kulikova O.M., Aleksandriiskii V.V., Koifman O.I. *Macroheterocycles* **2016**, *9*, 353–360, doi: 10.6060/mhc161067S.
56. Sheinin V.B., Kulikova O.M., Koifman O.I. *Macroheterocycles* **2018**, *11*, 363–370, doi: 10.6060/mhc181109S.
57. Sheinin V.B., Kulikova O.M. *Dyes Pigm.* **2021**, *194*, 109589, doi: 10.1016/j.dyepig.2021.109589.
58. Etter M.C. *Acc. Chem. Res.* **1990**, *23*, 120–126, doi: 10.1021/AR00172A005/ASSET/AR00172A005.FP.PNG_V03.
59. Sheinin V.B., Ivanova Y.B., Berezin B.D. *Russ. J. Coord. Chem.* **2002**, *28*, 149–151, doi: 10.1023/A:1014248604993/METRICS.
60. Sheinin V.B., Ivanova Y.B., Berezin B.D. *Russ. J. Gen. Chem.* **2002**, *72*, 1128–1131, doi: 10.1023/A:1020719303646/METRICS.
61. Sheinin V.B., Simonova O.R., Ratkova E.L. *Macroheterocycles* **2008**, *1*, 72–78, doi: 10.6060/mhc2008.1.72.
62. Sheinin V.B., Ratkova E.L., Mamardashvili N.Z. *J. Porphyrins Phthalocyanines* **2012**, *12*, 1211–1219, doi: 10.1142/ S1088424608000595.

63. Sutter T.P.G., Hambright P. *Inorg. Chem.* **1992**, *31*, 5089–5093, doi: 10.1021/ic00050a031.
64. Zenkevich E., Blaudeck T., Sheinin V., Kulikova O., Selyshchev O., Dzhagan V. *J. Mol. Struct.* **2021**, *1244*, 131239, doi: 10.1016/j.molstruc.2021.131239.
65. Gerola A.P., Semensato J., Pellosi D.S., Batistela V.R., Rabello B.R., Hioka N. *J. Photochem. Photobiol. A Chem.* **2012**, *232*, 14–21, doi: 10.1016/J.JPHOTOCHEM.2012.01.018.

Received 06.11.2023
Accepted 18.12.2023